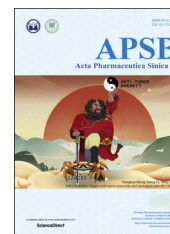




Chinese Pharmaceutical Association
Institute of Materia Medica, Chinese Academy of Medical Sciences

Acta Pharmaceutica Sinica B

www.elsevier.com/locate/apsb
www.sciencedirect.com



ORIGINAL ARTICLE

Dual-targeting and microenvironment-responsive micelles as a gene delivery system to improve the sensitivity of glioma to radiotherapy



Xiuxiu Jiao^{a,†}, Yuan Yu^{c,†}, Jianxia Meng^{d,†}, Mei He^a, Charles Jian Zhang^e, Wenqian Geng^a, Baoyue Ding^{b,*}, Zhuo Wang^{d,*}, Xueying Ding^{a,*}

^aDepartment of Pharmaceutics, Shanghai General Hospital, Shanghai Jiao Tong University of Medicine, Shanghai 200080, China

^bDepartment of Pharmaceutics, College of Medicine, Jiaying University, Jiaying 314000, China

^cDepartment of Pharmaceutical Sciences, School of Pharmacy, Second Military Medical University, Shanghai 200082, China

^dDepartment of Pharmacy, Changhai Hospital, Second Military Medical University, Shanghai 200082, China

^eDepartment of Pharmaceutical Sciences, College of Pharmacy, Western University of Health Sciences, Pomona, CA 91768, USA

Received 18 September 2018; received in revised form 12 November 2018; accepted 20 November 2018

KEY WORDS

Glioma-targeting;
Cell-penetrating peptides;
Microenvironment-responsive micelles;
Gene delivery;
Radiosensitizer

Abstract Dbait is a small double-stranded DNA molecule that has been utilized as a radiosensitizer to enhance the sensitivity of glioma to radiotherapy (RT). However, there is no effective drug delivery system to effectively overcome the blood–brain barrier (BBB). The aim of this study was to develop a gene delivery system by using the BBB and glioma dual-targeting and microenvironment-responsive micelles (ch-Kn(s-s)R8-An) to deliver Dbait into glioma for RT. Angiopep-2 can target the low-density lipoprotein receptor-related protein-1 (LRP1) that is overexpressed on brain capillary endothelial cells (BCECs) and glioma cells. In particular, due to upregulated matrix metalloproteinase 2 (MMP-2) in the tumor microenvironment, we utilized MMP-2-responsive peptides as the enzymatically degradable linkers to conjugate angiopep-2. The results showed that ch-Kn(s-s)R8-An micelles maintained a reasonable size

Abbreviations: Arg, arginine; ATCC, American Type Culture Collection; BBB, blood–brain barrier; BBTB, blood–brain tumor barriers; ch-KnR8-An, the non-cross-linked cholesterol-polylysine-polyarginine peptide core-shell polymer micelles modified with angiopep-2, $n = 3, 5, 7$; ch-Kn(s-s)R8-An, the disulfide cross-linked cholesterol-polylysine-polyarginine peptide core-shell polymer micelles modified with angiopep-2, $n = 3, 5, 7$; CMC, critical micelle concentration; DTSSP, 3,3'-dithiobis(sulfosuccinimidylpropionate); DTT, dithiothreitol; FBS, fetal bovine serum; GBM, glioblastoma multiforme; GSH, glutathione; KnR8, cholesterol-polylysine-polyarginine peptide, $n = 3, 5, 7$; Lys, lysine; MMP-2, matrix metalloproteinase 2; MWCO, molecular weight cutoff; PDI, polydispersity index; pDNA, plasmid DNA; PE, plating efficiency; PEI, polyethylenimine; RT, radiotherapy

*Corresponding authors.

E-mail addresses: lana_310@163.com (Baoyue Ding), wangzhuo@smmu.edu.cn (Zhuo Wang), dingxueying@126.com (Xueying Ding).

[†]These authors made equal contributions to this work.

Peer review under responsibility of Institute of Materia Medica, Chinese Academy of Medical Sciences and Chinese Pharmaceutical Association.

<https://doi.org/10.1016/j.apsb.2018.12.001>

2211-3835 © 2019 Chinese Pharmaceutical Association and Institute of Materia Medica, Chinese Academy of Medical Sciences. Production and hosting by Elsevier B.V. This is an open access article under the CC BY-NC-ND license (<http://creativecommons.org/licenses/by-nc-nd/4.0/>).

(80–160 nm) with a moderate distribution and a decreased mean diameter from the cross-linking as well as exhibited low critical micelle concentration (CMC) with positive surface charge, ranging from 15 to 40 mV. The ch-K5(s-s)R8-An/pEGFP showed high gene transfection efficiency *in vitro*, improved uptake in glioma cells and good biocompatibility *in vitro* and *in vivo*. In addition, the combination of ch-K5(s-s)R8-An/Dbait with RT significantly inhibited the growth of U251 cells *in vitro*. Thus, ch-K5(s-s)R8-An/Dbait may prove to be a promising gene delivery system to target glioma and enhance the efficacy of RT on U251 cells.

© 2019 Chinese Pharmaceutical Association and Institute of Materia Medica, Chinese Academy of Medical Sciences. Production and hosting by Elsevier B.V. This is an open access article under the CC BY-NC-ND license (<http://creativecommons.org/licenses/by-nc-nd/4.0/>).

1. Introduction

Glioblastoma multiforme (GBM) and malignant glioma are the most common primary malignant brain tumors^{1,2}. GBM is commonly treated with surgery followed by radiotherapy (RT) and chemotherapy. However, GBM cells are likely to infiltrate extensively into the surrounding normal brain tissue, making it difficult to completely eradicate the tumor by surgery³. Glioma is often resistant to radiotherapy (RT) due to its enhanced DNA repair activity⁴, while increased dose of RT may increase injury to cognition and other normal functions of the brain⁵. In addition, the blood–brain barrier (BBB) and blood–brain tumor barriers (BBTB) are also factors that may affect the efficacy of most therapeutic agents^{6,7}. Therefore, developing alternative approaches to overcome these problems and improve the therapeutic efficacy for glioma may be necessary.

Recent studies have shown that Dbait as a radiosensitizer combination with RT is effective for treating glioma, skin melanoma, colorectal cancer metastasis, and head and neck squamous cell carcinoma among others^{8–10}. Dbait is a new class of DNA double-strand breaks (DSBs) repair inhibitors consisting of a short double-stranded DNA molecule¹⁰. It can mimic DSBs to provide a “false” DNA damage signal and ultimately inhibit recruitment of many proteins involved in DSB repair pathways at the damage site^{11,12}. However, Dbait cannot easily enter cells or the BBB due to its relatively large size (20.153 kDa) and high negative charge content¹³. Thus, target delivery of Dbait into glioma cells is challenging.

To enhance the therapeutic efficacy, dual targeting delivery systems are designed to target both the BBB and glioma cells. Many types of receptors are overexpressed in brain capillary endothelial cells (BCECs) that form the BBB and on glioma cells, including insulin receptors, transferrin receptors and low-density lipoprotein receptor-related protein-1 (LRP1)^{14,15}. Angiopep-2, a member of the Kunitz domain-derived peptide family that can target the LRP1, exhibits a high transcytosis capacity and parenchymal accumulation as compared with transferrin, lactoferrin and avidin¹⁶. Angiopep-2 has been modified for use in delivery systems to facilitate penetration of the BBB and target glioma cells^{17–19}. In addition, tumor microenvironment-responsive release of nanoparticle (NP) constitutes an important strategy that can specifically deliver drugs or genes to tumors without causing drug-associated adverse effects on normal tissues^{18,20}. In particular, specific tumor microenvironment characteristics such as up-regulated matrix metalloproteinase 2 (MMP-2) activity and high glutathione concentrations in the cytosol of tumor cells are reported to promote the development of tumor microenvironment-responsive drug delivery systems^{21,22}.

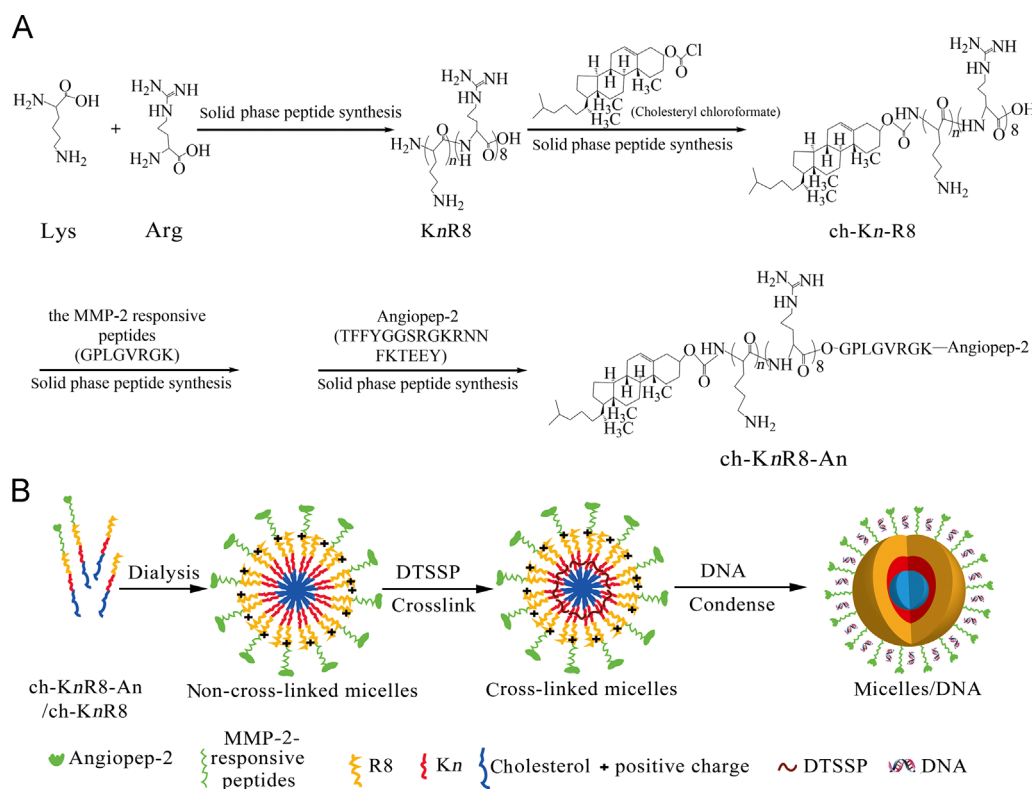
Recent studies have demonstrated that polypeptides and cell-penetrating peptides (CPPs) can serve as gene and drug delivery systems due to their inherent bioactivity, biodegradability and biocompatibility^{23–25}. Polyarginine molecules, which consist of 5–11 sequentially arranged arginines, have been shown to effectively penetrate the cell membrane, and R8 peptide can be internalized into cells most efficiently²⁵. However, studies^{26–28} showed that although CPPs could produce efficient cellular uptake *in vitro*, they could not accumulate in the target site *in vivo* effectively due to the lack of target cell specificity; as a result, the drug distributed in both tumor and healthy cells, producing undesirable effects during cancer treatment. To overcome this bottleneck, we chose the MMP-2 responsive peptide Gly-Pro-Leu-Gly-Val-Arg-Gly-Lys (GPLGVRGK) as an enzymatically degradable linker to conjugate angiopep-2 thereby reducing the cell-penetrating properties of CPPs in the circulation, and then expressed it intrinsically in the tumor. In the circulation, angiopep-2 could facilitate penetration of the BBB and accumulate at the tumor site, at which point the shielding effect would be eliminated upon the cleavage of the linker by MMP-2. Hence, the exposed CPPs subsequently internalized the delivery system into tumor cells.

In this study, we utilized the unique features of the tumor microenvironment to design novel dual-targeting and microenvironment-responsive micelles as gene delivery system (Scheme 1). In particular, we chose MMP-2-responsive peptides as the enzymatically degradable linkers to conjugate angiopep-2. The micelles are expected to effectively activate the target glioma and then further penetrate into the core of the tumor by exposing R8 following cleavage of the linker by MMP-2. To evaluate the tumor targeting and penetration abilities of the micelles, we first synthesized and characterized ch-Kn(s-s)R8-An, and examined the *in vitro* transfection efficiency, cytotoxicity, cellular uptake and BBB penetration. In addition, the effects and mechanisms of ch-K5(s-s)R8-An/Dbait in combination with RT on cell apoptosis were investigated to evaluate the antitumor activity of the micelles *in vitro*. Finally, acute toxicity and *in vivo* distribution of ch-K5(s-s)R8-An/pDNA in U251 orthotopic GBM-bearing were evaluated.

2. Materials and methods

2.1. Materials

Poly(ethylenimine) (PEI, branched, molecular weight 25 kDa) and dithiothreitol (DTT) were purchased from Sigma–Aldrich (St Louis, MO, USA). pDNA (pEGFP) was purchased from Shanghai



Scheme 1 (A) Synthesis of ch-KnR8-An. (B) Schematic diagram of the formation of ch-Kn(s-s)R8-An/pEGFP.

Innovation Biotechnology Co., Ltd. (Shanghai, China). Dbait was purchased from Wuhan GeneCreate Biological Engineering Co., Ltd. (Wuhan, China). Dulbecco's modified Eagle's medium (DMEM), fetal bovine serum (FBS), phosphate-buffered saline (PBS), trypsin, and penicillin–streptomycin solution (5 kU/mL) were purchased from Life Technologies Corporation (Carlsbad, CA, USA). Lysotracker Red was purchased from Beyotime biotechnology (Shanghai, China). 4',6-Diamidino-2-phenylindole (DAPI) was purchased from Cayman Chemical (Ann Arbor, MI, USA). YOYO-1 iodide was purchased from Thermo Fisher Scientific (Eugene, OR, USA). The Cell Counting Kit-8 (CCK-8) was purchased from Dojindo Molecular Technologies, Inc. (Nanjing, China). Annexin V-APC Apoptosis Analysis Kit was purchased from eBioscience (CA, USA). Dimethyl sulfoxide (DMSO) and pyrene (99%) were purchased from Sangon Biotech (Shanghai, China). 3,3'-Dithiobis(sulfosuccinimidylpropionate) (DTSSP) was purchased from J&K Chemical (Beijing, China). Recombinant-human MMP-2 proenzyme was obtained from Peprotech (Rocky Hill, NJ, USA). The peptides, cholesterol-KKKRRRRRRRRR, cholesterol-KKKKKRRRRRRRRR, and cholesterol-KKKKKKKRRRRRRRRR (ch-K3R8, ch-K5R8, and ch-K7R8), were designed by our group and synthesized by Ontores Bio (Hangzhou, China) at more than 95% purity. Angiopep-2 (TFYGGSRGKRNNFKTEEY) was also purchased from Ontores Bio. All other reagents were used as received.

The human malignant glioma cell line U251 was obtained from the Type Culture Collection of the Chinese Academy of Sciences (Shanghai, China). The human embryonic kidney cell line HEK293 was obtained from American Type Culture Collection (ATCC, Manassas, VA, USA). BCECs were kindly provided by Prof. Jianming Chen (Department of Pharmacy of the Second Military Medical University, Shanghai, China).

Male BALB/c nude mice (18–22 g) and male BALB/c mice (18–22 g) were purchased from the Department of Experimental Animals of the Second Military Medical University (Shanghai, China). All animal experiments were performed in accordance with the ethics and regulations of animal experimentation ethics and regulations of the Shanghai Jiao Tong University.

2.2. Synthesis and characterization of polymers

Schematic of synthesizing ch-KnR8 ($n = 3, 5$ and 7) graft copolymer is shown in [Scheme 1 A](#) using the F-moc-solid phase peptide synthesis method²⁹. Lysine-arginine peptide (KnR8) was synthesized using the F-moc-solid phase peptide synthesis method. Second, we coupled cholesterol with the N-terminus of the lysine to obtain ch-KnR8. In addition, we chose the MMP-2 responsive peptide (GPLGVRGK) as the enzymatically degradable linker for conjugation to angiopep-2 using the F-moc-solid phase peptide synthesis method to obtain the angiopep-2-modified graft copolymer (ch-KnR8-An, $n = 3, 5$ and 7). The products were then purified by reverse-phase high-performance liquid chromatography. The precise molecular weight of ch-KnR8 and ch-KnR8-An ($n = 3, 5$ and 7) were measured using matrix-assisted laser desorption/ionization–time-of-flight-mass spectrometry (MALDI-TOF-MS) (Bruker Daltonik GmbH, Bremen, HB, Germany).

2.3. Preparation and characterization of micelles/DNA

2.3.1. Preparation and characterization of blank micelles

The polymeric micelles with shell-specific disulfide cross-links were prepared by a membrane dialysis method and a subsequent shell cross-linking reaction ([Scheme 1 B](#))^{30,31}. The ch-KnR8

($n = 3, 5$ and 7) polymer (10 mg) was dissolved in DMSO. The solution was dialyzed against 1 L of deionized water for 48 h using a dialysis membrane bag with a molecular weight cut-off (MWCO) of 3000 Da (Pierce Co, Rockford, IL, USA). The blank non-cross-linked micelles (ch- $KnR8$, ch- $KnR8$ -An, $n = 3, 5$ and 7) were then collected. Next, DTSSP used as a disulfide-containing cross-linking agent was added to the solution at the feed molar ratio of [DTSSP]:[Lys] = 1:1. The reaction was maintained for 4 h at pH 8.0 and the solution was then dialyzed for 4 h to remove residual DTSSP. For the brain-targeting micelle preparation, 50% (mol of total copolymers) ch- $KnR8$ -An was added to the copolymer-DMSO solution. Subsequently, blank cross-linked micelles (ch- $Kn(s-s)R8$, ch- $Kn(s-s)R8$ -An, $n = 3, 5$ and 7) were obtained after lyophilization. The specific absorption peaks of the disulfide bond range between 240 and 300 nm of different micelles was detected by ultraviolet and visible spectrophotometry (UV 2450/2550, Shimadzu, Japan). The particle size and zeta potential of blank micelles were measured in a PBS solution (pH 7.4) by dynamic light scattering (Zetasizer Nano ZS90, Malvern Instruments, Malvern, UK). The morphology of the ch- $Kn(s-s)R8$ -An was examined using a transmission electron microscope (TEM) (Hitachi, Tokyo, Japan) at an acceleration voltage of 75 kV.

2.3.2. Critical micelle concentration (CMC)

The CMC of micelles was determined using a pyrene fluorescence method as described previously³². Briefly, pyrene solution (6×10^{-5} mol/L in acetone) was transferred into a series of volumetric flasks and the acetone was evaporated under a gentle nitrogen gas stream for 4 h at room temperature. The ch- $KnR8$ -An and ch- $Kn(s-s)R8$ -An solutions in a series of concentrations ranging from 1×10^{-5} to 2 mg/mL in deionized water were added into each flask with a final pyrene concentration of 6×10^{-6} mol/L. The fluorescence spectrum was obtained using a F-7000 fluorescence spectrometer (Hitachi, Japan). Intensity ratios of the first (374 nm) to the third (384 nm) vibronic peaks (I_1/I_3) were plotted as a logarithm function of the micelles concentration. The CMC value was taken from the intersection of the tangent to the curve at the inflection with the horizontal tangent through the points at low concentrations.

2.3.3. Stability of ch- $Kn(s-s)R8$ -An

The kinetic stability of ch- $Kn(s-s)R8$ -An ($n = 3, 5$ and 7) micelles were studied in PBS (pH 7.4) with or without 10% FBS under mild stirring at 37 °C. The particle size and zeta potential of micelles were monitored at 0, 1, 2, 4, 8, 12 and 24 h, respectively.

2.3.4. Preparation and characterization of micelles/DNA

pEGFP was used as a model plasmid. The ch- $Kn(s-s)R8$ -An ($n = 3, 5$ and 7) micelles were mixed with pEGFP plasmid (60 μ L per 2 μ g DNA) at different N/P ratios from 1:1 to 15:1 in 1 mL PBS (pH 7.4). The particle size and zeta potential of ch- $Kn(s-s)R8$ -An/pEGFP at different N/P ratios were measured in a PBS solution (pH 7.4) by dynamic light scattering.

2.4. Agarose gel electrophoresis

The ability of the micelles to condense pDNA was determined by agarose gel electrophoresis. The ch- $Kn(s-s)R8$ -An/pEGFP ($n = 3, 5$ and 7) was prepared at different N/P ratios (0–5). After 30 min of incubation the samples were analyzed on a 1.0% agarose gel by

staining with GelRed™ fluorescent dye and Tris-acetate EDTA buffer for 40 min at 4 °C. Then, the samples were electrophoresed at 100 V for 40 min. pDNA was visualized using a UV transilluminator. To compare the stability of the ch- $Kn(s-s)R8$ -An/pEGFP under reductive environments, ch- $Kn(s-s)R8$ -An/pEGFP at different N/P ratios in the presence of 100-fold DTT (mole ratio to ch- $KnR8$ -An monomer) was analyzed using agarose gel electrophoresis. pEGFP bands were visualized under UV light. ch- $Kn(s-s)R8$ -An/pEGFP stability was evaluated using a heparin competition assay. The ch- $Kn(s-s)R8$ -An/pEGFP was prepared at an N/P ratio of 10. Then, increasing amounts of heparin were added to the micelles/pEGFP. After treatment for 1 h, the samples were assessed using agarose gel electrophoresis under the same conditions.

2.5. Gene transfection assay

HEK293 and U251 cells were seeded in 24-well plates at a density of 2×10^5 and 5×10^4 cells/well, respectively. After 24 h, when the cells achieved 70%–80% confluence, the culture medium was removed. Cells were exposed to fresh serum-free culture medium containing ch- $Kn(s-s)R8$ -An/pEGFP with different N/P ratios and incubated for another 6 h, after which the medium was replaced with DMEM containing 10% FBS and cells were incubated an additional 42 h. The expression of pEGFP in cells was observed by fluorescence microscopy (Leica, CMS, GmbH, Germany) and quantified by flow cytometry (Becton Dickinson, San Jose, CA, USA). Naked pEGFP and bPEI-25K/pEGFP were used as controls. The experiment was repeated three times.

2.6. Cytotoxicity assay

The cytotoxicity of the ch- $Kn(s-s)R8$ -An/pEGFP ($n = 3, 5$ and 7) toward BCECs and U251 cells was evaluated by CCK-8 assay. BCECs and U251 cells in 100 μ L DMEM containing 10% FBS were seeded in 96-well plates at a density of 8000 cells/well. After 24 h, the cells were transfected as described above and the medium was replaced with fresh culture medium containing various concentrations of ch- $Kn(s-s)R8$ -An/pEGFP at an N/P ratio of 10. The final concentrations of the polymer ranged from 5–200 μ g/mL. After 24 h, the medium was then replaced by 90 μ L of fresh complete medium and 10 μ L of CCK-8 solution. The cells were incubated for an additional hour. The absorbance of each well was measured at 450 nm using a microplate reader (Thermo Fisher Scientific, Waltham, MA, USA). The absorbance of untreated cells was set at 100%, and cell viability was expressed as the percentage relative to the absorbance of the untreated cells. bPEI-25K/pEGFP were used as controls. The experiment was repeated four times.

2.7. In vitro cellular uptake assay

2.7.1. Cellular uptake determined by flow cytometry

HEK293 cells and BCECs were seeded in 12-well plates at a density of 3×10^5 cells per well. Prior to preparation of the micelles/pEGFP at an N/P ratio of 10, pEGFP was labeled with YOYO-1 for 30 min. After replacing the culture medium, the ch- $K5(s-s)R8$ -An/pEGFP-YOYO-1 solution was added to HEK293 cells and BCECs, with a final pEGFP-YOYO-1 concentration of 75 nmol/L. After 3 h of incubation, the cells were trypsinized, centrifuged, washed, and resuspended in PBS. The fluorescence intensity of cells was analyzed on a flow cytometer. bPEI-25k/

pEGFP-YOYO-1, ch-K5(s-s)R8/pEGFP-YOYO-1 and pEGFP-YOYO-1 were used as controls. The experiment was replicated three times.

2.7.2. BBB penetration *in vitro*

The transportation study was performed using an *in vitro* BBB model that was established using the method described previously. BCECs in 500 μ L DMEM containing 10% FBS were seeded at a density of 1×10^6 cells/mL on the upper side of 24-transwell plate filters. Then, 1 mL DMEM-free FBS was added in the lower side of the 24-transwell plate filters. The culture medium was replaced every 2 days. After 4 days, U251 cells were seeded in the lower side of the 24-transwell plate filters at a density of 2×10^5 cells/well and grown overnight. To evaluate their ability as carriers across the BBB, bPEI-25k/pEGFP-YOYO-1, ch-K5(s-s)R8/pEGFP-YOYO-1, and ch-K5(s-s)R8-An/pEGFP-YOYO-1 were added into the corresponding insert. In addition, to evaluate the effect of MMP-2 on U251 cellular uptake, MMP-2 was added into the lower side (the size and TEM images of ch-K5(s-s)R8-An micelles after MMP-2 treated was measured by the methods mentioned earlier) and ch-K5(s-s)R8-An/pEGFP-YOYO-1 were added into the upper side. After 12 h of incubation, the fluorescence intensity of cells was analyzed using flow cytometry. The experiment was replicated three times.

2.7.3. Confocal laser scanning microscopy (CLSM)

To investigate the cellular uptake profiles of micelles, 1×10^5 cells/well U251 cells were seeded onto sterilized microscope cover slips placed in 24-well plate and incubated for 24 h. Seeded cells were then treated with naked pEGFP, bPEI-25K/pEGFP-YOYO-1, ch-K5(s-s)R8/pEGFP-YOYO-1 or ch-K5(s-s)R8-An/pEGFP-YOYO-1 and incubated for 1, 2 or 3 h (untreated cells were used as control). Afterwards, the cells were washed with PBS and incubated with LysoTracker red for 30 min. Then the cells were washed with PBS, fixed in 4% paraformaldehyde, treated with DAPI for staining of the nucleus, sealed with mounting medium, and imaged using a confocal laser scanning microscope (TCS SP8, Leica, Wetzlar, Germany).

2.8. Radiosensitization effects of ch-K5(s-s)R8-An/Dbait

2.8.1. CCK-8 assay

A CCK-8 assay was used to compare the cytotoxicity of various treatments at different radiation doses. The preparation of ch-K5(s-s)R8-An/Dbait was similar to ch-K5(s-s)R8-An/pEGFP at an N/P ratio of 10. U251 cells in 100 μ L DMEM containing 10% FBS and an appropriate amount of MMP-2 were seeded in 96-well plates at a density of 8000 cells/well. After 24 h, cells were treated with ch-K5(s-s)R8-An, Dbait and ch-K5(s-s)R8-An/Dbait. After 6 h, cells were irradiated with 0, 2, 4, 8 or 12 Gy, respectively (dose rate = 0.3 Gy/min). After 48 h, cell viability was determined by CCK-8 assay.

2.8.2. Colony formation assay

The X-ray radiation treatment was performed at increasing doses from 0 to 4 Gy, as reported previously. Briefly, U251 cells in DMEM containing 10% FBS and an appropriate amount of MMP-2 were seeded into 6-well plates at 400 cells/mL/2 mL. After 24 h, cells were treated with ch-K5(s-s)R8-An, Dbait and ch-K5(s-s)R8-An/Dbait. After 6 h, cells were irradiated with 0, 2 or 4 Gy, respectively (dose rate = 0.3 Gy/min). About 14 days later, cell

clones were fixed with ice-cold acetic acid and incubated for 15 min, then stained with crystal violet. All colonies with over 50 cells were counted and the data were analyzed using Graph Pad Prism software. Untreated cells were considered as controls. The plating efficiency (PE) was calculated by dividing the number of colonies by the number of cells plated.

2.8.3. Cell apoptosis assay

In order to determine the rate of apoptosis, U251 cells in DMEM containing 10% FBS and an appropriate amount of MMP-2 were seeded in 12-well plates at a density of 1.5×10^5 cells/well. After 24 h, cells were treated with ch-K5(s-s)R8-An, Dbait and ch-K5(s-s)R8-An/Dbait. After 6 h, cells were irradiated with 2 Gy (dose rate = 0.3 Gy/min). After 48 h, the cells were washed twice with ice-cold PBS, trypsinized, centrifuged and then re-suspended in cold binding buffer. The cells were stained with Annexin V-APC and propidium iodide (PI), followed by incubation in the dark for 10 min. A total of at least 10,000 cells from each sample were analyzed using an analytical flow cytometer (FACSCalibur; BD Biosciences, UK). Untreated cells were used as controls. The tests were carried out in triplicate.

2.8.4. Western blot

U251 cells were seeded and treated as described above in the cell apoptosis assay. After 48 h, cells were harvested and resuspended in RIPA lysis buffer with protease inhibitor and phosphatase inhibitor, followed by incubation on ice for 30 min. The lysates were centrifuged at 12,000 rpm (Thermo ST40, USA) for 10 min at 4 °C, the supernatants were collected and examined for protein concentrations using the BCA protein assay kit (Thermo, USA). Proteins were separated by SDS-PAGE, electro-transferred to polyvinylidene fluoride membrane (Millipore, USA), and blocked using 5% non-fat dried milk at RT for 1 h. Membranes were incubated overnight at 4 °C with the following primary antibodies: γ -H2AX (Abcam, UK), DNA-PKcs (Bioworld, China), phosphorylated p53 (Ser15) (Abcam, UK) and GAPDH (Bioworld, China). After washing, membranes were then incubated with HRP-conjugated secondary antibodies (Cell Signaling, USA) for 1 h at room temperature. Visualization was performed as previously described.

2.9. *In vivo* biodistribution

Micelles/pEGFP-YOYO-1 were used to investigate the distribution of NPs in U251 orthotopic GBM-bearing nude mice, as described previously. Male nude mice were divided randomly into three groups. Each mouse was anesthetized with 1% pentobarbitalum natrium and placed in a stereotaxic apparatus. U251 cells (1×10^5 cells/5 μ L) were then injected into the right brain of each mouse (1 mm lateral to bregma and 3.0 mm deep from the dura). Two weeks later, tumor-bearing mice were injected intravenously through the tail vein with 200 μ L of PBS, YOYO-1, ch-K5(s-s)R8/pEGFP-YOYO-1, or ch-K5(s-s)R8-An/pEGFP-YOYO-1 at a dose of 50 mg pEGFP per mouse. After 24 h, mice were sacrificed and the principal organs (heart, liver, spleen, lung, kidneys, and brain) were carefully removed. Biodistribution was evaluated using *in vivo* fluorescence imaging (Xenogen IVIS-200, Caliper Life Sciences, Hopkinton, MA, USA).

2.10. *In vivo* safety assay

BALB/c mice were divided randomly into 2 groups and injected with PBS and blank ch-K5(s-s)R8-An micelles through the tail

vein at a dose of 30 mg/kg every 2 days totaling 4 injections. The mice were sacrificed 24 h after the last injection to excise the heart, liver, spleen, lung, kidney, and brain. The excised organs were fixed in 4% paraformaldehyde, and then subjected to hematoxylin and eosin (H&E) staining.

2.11. Statistical analysis

All values are presented as the means \pm standard deviation (SD). One-way analysis of variance (ANOVA) was used for the statistical analysis. The differences were considered significant for $*P < 0.05$.

3. Results

3.1. Synthesis and characterization of polymers

As a self-assembling block copolymer for the core-shell polymer micelles, the ch-KnR8 ($n = 3, 5$ and 7) and ch-KnR8-An ($n = 3, 5$ and 7) copolymers were synthesized via the F-moc-solid phase peptide synthesis method (Scheme 1A) and a subsequent purification process. The copolymers were synthesized at 95% purity and the precise molecular weight of ch-K5R8 and ch-K5R8-An are shown in ESI Supporting Information Table S1. The MALDI-TOF-MS data demonstrate that ch-KnR8-An ($n = 3, 5$ and 7) was successfully synthesized.

3.2. Preparation and characterization of micelles/DNA

3.2.1. Preparation and characterization of blank micelles

Ch-KnR8 self-assembled and formed a core-shell-corona polymer micelle with three well-defined distinct domains: the inner hydrophobic cholesterol core, the cationic Kn middle shell, and the cationic R8 outer corona. For cross-linked micelle formation, DTSSP with activated bifunctional NHS groups could react with amino groups of the pLys segment to form intramolecular disulfide linkages³¹. Cross-linked micelles ch-Kn(s-s)R8-An ($n = 3, 5$ and 7) were confirmed to contain disulfide bonds as demonstrated with an absorption peak of 270 nm (Supporting Information Fig. S1). The micelle size and zeta potential are shown in Table 1. The micelles maintained a reasonable size (80–160 nm) with a moderate distribution and a decreased mean diameter from the cross-linking, which may facilitate the accumulation of micelles in tumor tissues. The zeta potential of the blank micelles was different, ranging from 15 to 40 mV. Notably, after the cross-linking, the values of the positive zeta potential of ch-KnR8 and ch-KnR8-An were decreased. Among the micelles, ch-K5(s-s)R8-An is presented as an example to show an appropriate size and zeta potential (Fig. 1A and B), with a particle size and zeta potential of 119.5 ± 4.31 nm and 25.0 ± 2.70 mV, respectively. Fig. 1A presents the TEM images of the ch-K5(s-s)R8-An micelle. It shows that the micelle assumed a spherical morphology and almost homogeneous distribution.

3.2.2. The CMC of micelles

To confirm the formation of micelles self-assembled from the ch-KnR8-An block copolymer, the CMC values of ch-KnR8-An and ch-Kn(s-s)R8-An ($n = 3, 5$ and 7) micelles were measured by fluorescence spectroscopy. As the micelle concentration increased, the intensity ratio exhibited a substantial decrease at a certain

concentration, suggesting that pyrene molecules were incorporated into the hydrophobic core region during micelle formation. Therefore, CMC values were determined from the crossover point at the low concentration. As shown in Fig. 1C and D, the CMC values of ch-KnR8-An and ch-Kn(s-s)R8-An ($n = 3, 5$ and 7) micelles were approximately 0.00794, 0.00891, 0.0138, 0.00750, 0.00116 and 0.00284 mg/mL, respectively. The cross-linked micelles had lower CMC values compared with the non-cross-linked ones and K5(s-s)R8-An had the lowest CMC value, indicating that they had the best stability in solution.

3.2.3. Stability of ch-Kn(s-s)R8-An

The kinetic stability of ch-Kn(s-s)R8-An micelles were further assessed in PBS (pH 7.4) with or without 10% FBS. As shown in Supporting information Fig. S2, ch-Kn(s-s)R8-An micelles maintained their size in a range of 90–160 nm and zeta potential in a range of 10–40 mV in PBS (pH 7.4) with or without 10% FBS for up to 24 h, and there is no significant differences between two kinds of medium, indicating that the micelles are stable in serum.

3.2.4. Preparation and characterization of micelles/DNA

In the present study, the particle size and zeta potential of ch-Kn(s-s)R8-An/pEGFP ($n = 3, 5$ and 7) with different N/P ratios are shown in Fig. 1E. All ch-Kn(s-s)R8-An/pEGFP carried a positive surface charge with zeta potential ranging from 10 to 30 mV when the N/P ratio was higher than 5. Fig. 1F shows that the particle size of the ch-Kn(s-s)R8-An/pEGFP was less than 200 nm at an N/P ratio higher than 2.5. When the N/P ratio was higher than 5, most ch-Kn(s-s)R8-An/pEGFP had a higher zeta potential and a smaller particle size.

3.3. Agarose gel electrophoresis

Fig. 1G shows the result of agarose gel electrophoresis for pDNA binding affinity for ch-Kn(s-s)R8-An/pEGFP ($n = 3, 5$ and 7). pEGFP was retarded completely at an N/P ratio of 5, 3, and 2 for ch-Kn(s-s)R8-An/pEGFP ($n = 3, 5$ and 7) respectively, whereas pEGFP was not completely retarded at an N/P ratio of 5 for ch-K3R8-An/pEGFP and was retarded at an N/P ratio of 5 and 3 for ch-KnR8-An/pEGFP ($n = 5, 7$), indicating that the binding affinity of ch-Kn(s-s)R8-An was improved by disulfide bond

Table 1 Sizes and zeta potentials of the different micelles.

Group	Mean size ^a (nm)	Zeta potential ^b (mV)
ch-K3R8	93.9 \pm 1.95	20.2 \pm 3.87
ch-K3(s-s)R8	87.5 \pm 5.87	16.0 \pm 2.67
ch-K3R8-An	133.8 \pm 4.87	22.1 \pm 5.19
ch-K3(s-s)R8-An	100.2 \pm 0.45	19.0 \pm 3.39
ch-K5R8	103.1 \pm 2.47	29.8 \pm 4.12
ch-K5(s-s)R8	95.4 \pm 5.02	23.4 \pm 3.82
ch-K5R8-An	139.5 \pm 8.81	30.7 \pm 6.34
ch-K5(s-s)R8-An	119.5 \pm 4.31	25.0 \pm 2.70
ch-K7R8	143.0 \pm 7.94	37.5 \pm 4.35
ch-K7(s-s)R8	128.4 \pm 4.78	33.9 \pm 3.07
ch-K7R8-An	154.5 \pm 6.33	41.4 \pm 4.98
ch-K7(s-s)R8-An	136.3 \pm 1.94	35.3 \pm 2.02

Data are shown as the means \pm standard deviation ($n = 3$).

^aMean hydrodynamic diameters at 25 °C.

^bEstimated at pH 7.4 at 25 °C.

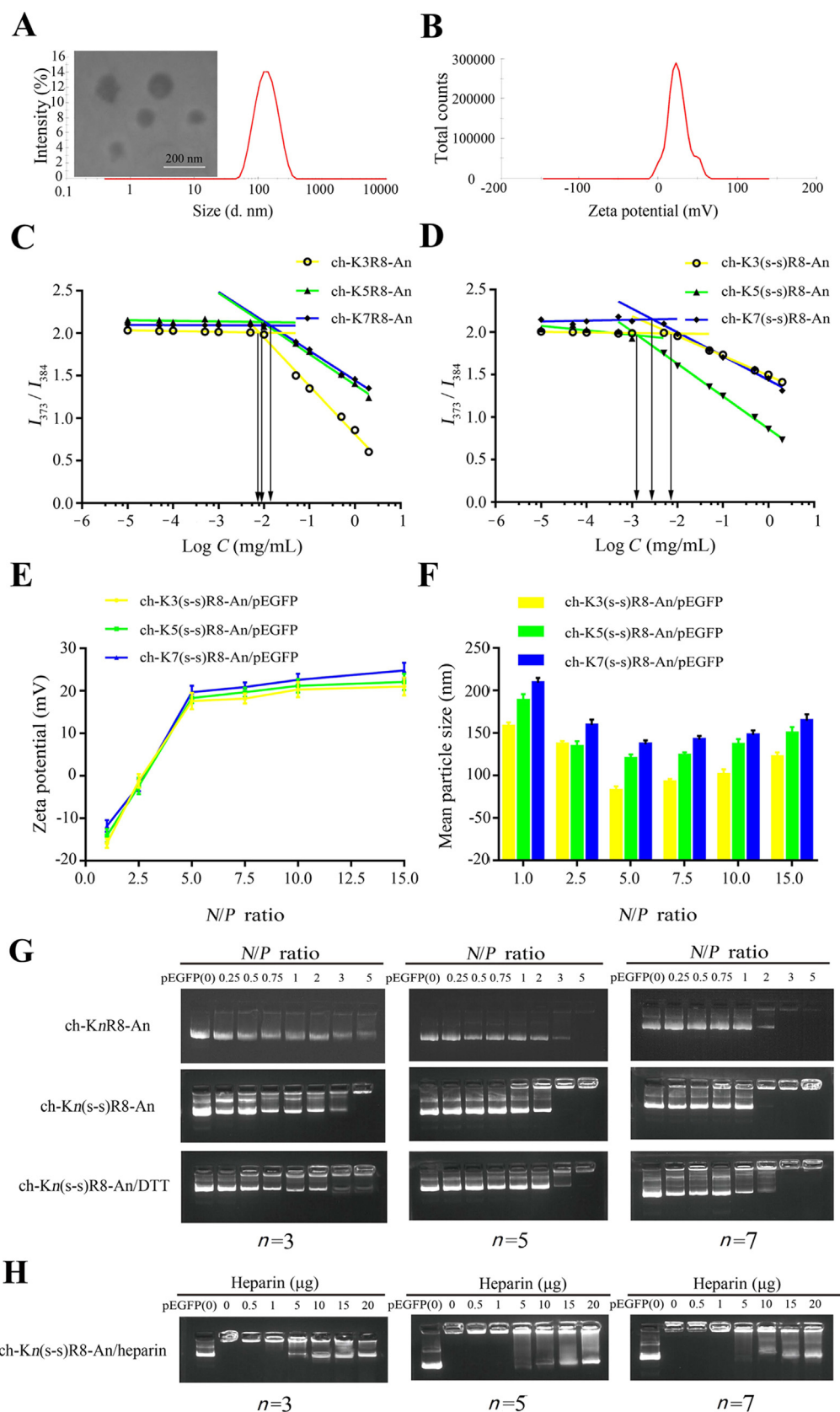


Figure 1 Characterization of micelles and micelles/pEGFP. (A) Particle size and TEM images of ch-K5(s-s)R8-An micelles. Scale bar, 200 nm. (B) Zeta potential of ch-K5(s-s)R8-An micelles. (C) Variation of intensity ratio (I_{373}/I_{384}) versus the logarithm of ch-KnR8-An concentrations. (D) Variation of intensity ratio (I_{373}/I_{384}) versus the logarithm of ch-Kn(s-s)R8-An concentrations. (E) Zeta potential of micelles/pEGFP at various N/P ratios. (F) Particle size of micelles/pEGFP at various N/P ratios. (G) Agarose gel electrophoresis of the pEGFP binding affinity for ch-KnR8-An and ch-Kn(s-s)R8-An at various N/P ratios and in the presence of reducing agent (DTT). (H) Heparin was used to evaluate the stabilities of the ch-Kn(s-s)R8-An/pEGFP at an N/P ratio of 10.

cross-linking. To verify this finding, DTT was used as a reducing agent to break the disulfide bond³³. As shown in Fig. 1G, ch-Kn(s-s)R8-An/pEGFP ($n = 3, 5$ and 7) had weaker pEGFP binding affinity in the presence of DTT due to depolymerization of ch-Kn(s-s)R8-An. The stability of the ch-Kn(s-s)R8-An/pEGFP ($n = 3, 5$ and 7) was measured by heparin competition assays (Fig. 1H). Increasing amounts of heparin were added to the ch-Kn(s-s)R8-An/pEGFP ($n = 3, 5$ and 7) solution and dissociation of the ch-Kn(s-s)R8-An/pEGFP ($n = 3, 5$ and 7) was measured by gel electrophoresis. Ch-K3(s-s)R8-An released pEGFP in the presence of $5 \mu\text{g}$ heparin whereas ch-K5(s-s)R8-An and ch-K7(s-s)R8-An released pEGFP upon the addition of $10 \mu\text{g}$ heparin. In addition, with the amount of heparin increasing, pEGFP was released to a greater degree. These results suggest that ch-K5(s-s)R8-An/pEGFP and ch-K7(s-s)R8-An/pEGFP were more stable than ch-K3(s-s)R8-An/pEGFP.

3.4. Gene transfection assay

Gene transfection efficiency of the micelles in HEK293 and U251 cells was evaluated using pEGFP as the model plasmid. Naked pEGFP and bPEI-25K were used as controls. The result showed that the gene transfection efficiency was dependent on the N/P ratio as observed for HEK293 cells (Fig. 2A). As shown in Fig. 2A, naked pEGFP exhibited the lowest gene transfection efficiency, and ch-Kn(s-s)R8-An/pEGFP ($n = 5$ and 7) showed significantly higher EGFP fluorescence intensities than ch-K3(s-s)R8-An/pEGFP at N/P ratios of $5, 7.5, 10$, and 15 . The fluorescence intensity of ch-Kn(s-s)R8-An/pEGFP ($n = 5$ and 7) at an N/P ratio of 10 was comparable with that of bPEI-25K/pEGFP. In addition, the EGFP fluorescence intensity following transfection by ch-Kn(s-s)R8-An/pEGFP ($n = 5$ and 7) and bPEI-25K/pEGFP at an N/P ratio of 10 in U251 cells was also higher than that of ch-K3(s-s)R8-An/pEGFP and naked pDNA (Fig. 2B). Flow cytometry assay determination of the mean fluorescence intensity in U251 cells also confirmed this tendency (Fig. 2C), most probably because of the enhanced gene compression of the ch-Kn(s-s)R8-An/pEGFP ($n = 5$ and 7)³⁴. Notably, ch-Kn(s-s)R8-An/pEGFP ($n = 5$ and 7) showed optimal gene transfection efficiency at an N/P ratio of 10 .

3.5. Cytotoxicity assay

The cytotoxicity of the ch-Kn(s-s)R8-An/pEGFP ($n = 3, 5$ and 7) and bPEI-25K/pEGFP in BCECs and U251 cells is shown in Fig. 2D and E. Ch-Kn(s-s)R8-An/pEGFP ($n = 3, 5$ and 7) showed significantly lower cytotoxicity than the bPEI-25K/pEGFP ($P < 0.05$) at concentrations of $5\text{--}200 \mu\text{g/mL}$. No significant cytotoxicity was observed over a 24-h transfection period with ch-K3(s-s)R8-An/pEGFP and ch-K5(s-s)R8-An/pEGFP at concentrations of $0\text{--}100 \mu\text{g/mL}$. The viability of both cell lines remained above 80% , demonstrating the biocompatibility of these micelles/pEGFP with BCECs and U251 cells. However, cell viability decreased to approximately 60% in BCECs and 30% in U251 cells for ch-K7(s-s)R8-An/pEGFP at a concentration of $100 \mu\text{g/mL}$ when compared with untreated cells. In addition, cell viability decreased to approximately 30% in both cell lines for bPEI-25K/pEGFP at a concentration of $30 \mu\text{g/mL}$. On BCECs cells, the IC_{50} values of bPEI-25K/pEGFP and ch-K7(s-s)R8-An/pEGFP group were 20 and $150 \mu\text{g/mL}$, respectively. On U251 cells, the IC_{50} values of bPEI-25K/pEGFP and ch-K7(s-s)R8-An/pEGFP were

about 8 and $60 \mu\text{g/mL}$, respectively. The higher cytotoxicity of the ch-K7(s-s)R8-An/pEGFP may be due to the high charge density. Based on the above results, ch-K5(s-s)R8-An/pEGFP was selected for further study.

3.6. In vitro cellular uptake assay

3.6.1. Cellular uptake determined by flow cytometry

The *in vitro* internalization efficiency was evaluated using a cellular uptake study. As shown in Fig. 3A, cellular uptake efficiency was significantly higher for ch-K5(s-s)R8 than that for pEGFP, bPEI-25K, and ch-K5(s-s)R8-An in HEK293 cells. Specifically, mean fluorescence intensity of ch-K5(s-s)R8/pEGFP was approximately 2.50-fold and 2.15-fold higher than that of ch-K5(s-s)R8-An/pEGFP and bPEI-25K/pEGFP, respectively (both $P < 0.05$). At the same time, cellular uptake efficiency of ch-K5(s-s)R8/pEGFP and ch-K5(s-s)R8-An/pEGFP was significantly higher than that for bPEI-25K/pEGFP and naked pEGFP in BCECs (Fig. 3B). Here, mean fluorescence intensity of ch-K5(s-s)R8/pEGFP and ch-K5(s-s)R8-An/pEGFP was approximately 3.17-fold and 3.36-fold higher than that of bPEI-25K/pEGFP ($P < 0.05$). These flow cytometric analysis results indicate that the cholesterol hydrophobic moiety enhanced the membrane affinity for the micelles/pEGFP. In addition, compared with the non-targeting ch-K5(s-s)R8/pEGFP, the targeting ch-K5(s-s)R8-An/pEGFP entered BCECs much more efficiently as represented by significantly intensified intracellular fluorescence in BCECs which was the opposite for HEK293 cells. These findings may be due to surface modifications of the micelles. Specifically, non-targeting micelles with a polyarginine shell were positively charged and could better penetrate the cell membrane, albeit not selectively. However, Angiopep-2 recognized and bound to LPR1 that was overexpressed on the BCECs, thus retaining more pEGFP in the BCECs.

3.6.2. BBB penetration in vitro

Transport experiments were performed to examine the permeability of micelles using an *in vitro* BBB model (Fig. 3C), and analyze the effect of Angiopep-2 on ch-K5(s-s)R8-An transcytosis across the BBB. Fig. 3D shows the results of the flow cytometric analysis of micelles/pDNA across the BBB and cellular uptake of micelles/pDNA in U251 cells over a 12 h period. The mean fluorescence intensity of both ch-K5(s-s)R8/pEGFP-YOYO-1 and ch-K5(s-s)R8-An/pEGFP-YOYO-1 in U251 cells was higher than that of bPEI-25K/pEGFP-YOYO-1 ($P < 0.05$), indicating that cholesterol peptide micelles enhanced the BBB penetration efficiency. In addition, the non-targeting ch-K5(s-s)R8/pEGFP-YOYO-1 showed significant cellular uptake efficiency due to efficient internalization of R8^{35,36}. The uptake efficiency of ch-K5(s-s)R8-An/pEGFP-YOYO-1 was not ideal (62.4% relative to ch-K5(s-s)R8/pEGFP-YOYO-1). However, the uptake efficiency of ch-K5(s-s)R8-An/pEGFP-YOYO-1 increased by 102.8% relative to ch-K5(s-s)R8/pEGFP-YOYO-1 and 164.9% relative to ch-K5(s-s)R8-An/pEGFP-YOYO-1 after treatment with MMP-2 to cleave the linkers exposing R8 to imitate a tumor microenvironment. The BBB penetration of ch-K5(s-s)R8-An/pEGFP-YOYO-1 was not significantly enhanced by Angiopep-2 conjugation, whereas treatment of ch-K5(s-s)R8-An/pEGFP-YOYO-1 with MMP-2 favorably impacted their efficient internalization. In addition, the particle size and TEM image of ch-K5(s-s)R8-An after MMP-2 treated are showed in Supporting Information Fig. S3, indicating that ch-K5(s-s)R8-An was degraded. These results further confirmed that ch-K5(s-s)R8-An/pEGFP-YOYO-1 was able to target

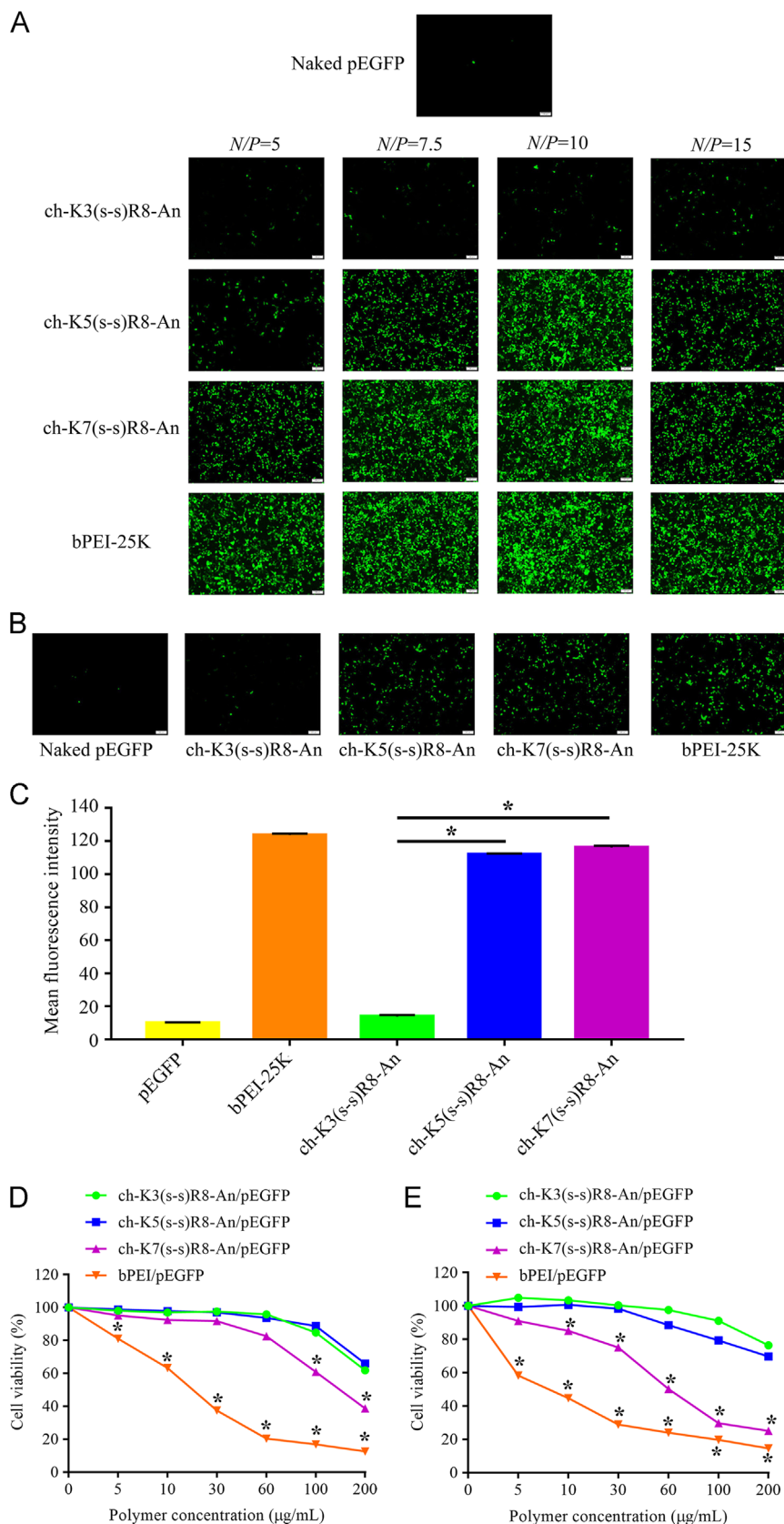


Figure 2 *In vitro* transfection efficiency and cytotoxicity of micelles/pEGFP. (A) Fluorescent images of the transfection efficiency of micelles/pEGFP at various *N/P* ratios of 5, 7.5, 10 and 15 in HEK293 cells. (B) Fluorescent images of the transfection efficiency of micelles/pEGFP at an *N/P* ratio of 10 in U251 cells. (C) Quantitative analysis of transfection efficiency for micelles/pEGFP at an *N/P* ratio of 10 in U251 cells using flow cytometry. (D) Cytotoxicity of micelles/pEGFP toward BCECs for 24 h. (E) Cytotoxicity of micelles/pEGFP toward U251 cells for 24 h. Scale bar, 100 μm (mean \pm SD, $n = 3$; * $P < 0.05$).

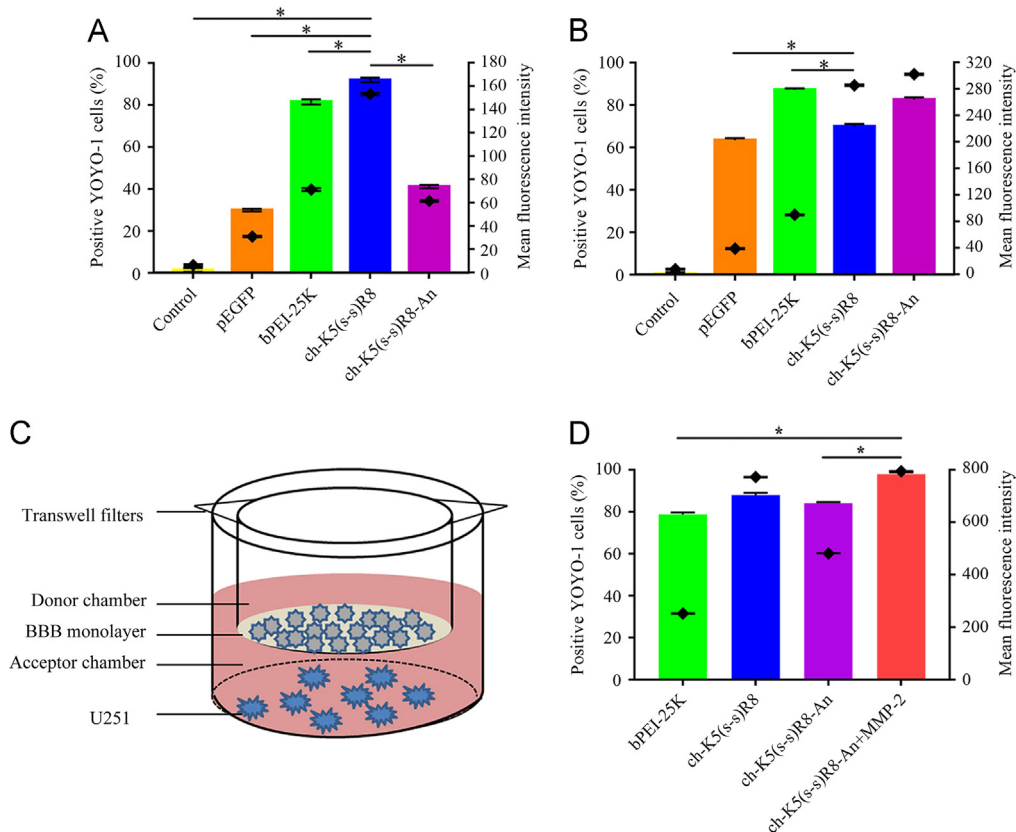


Figure 3 Intracellular uptake of pEGFP-YOYO-1. (A) Intracellular uptake of pEGFP-YOYO-1 based on different micelles at an *N/P* ratio of 10 in HEK293 cells after 3 h of transfection. (B) Intracellular uptake of pEGFP-YOYO-1 based on different micelles at an *N/P* ratio of 10 in BCECs after 3 h of transfection. (C) Schematic illustration of the *in vitro* BBB model. (D) The penetration effect of pEGFP-YOYO-1 based on different micelles at an *N/P* ratio of 10 in U251 cells. Diamonds (◆) indicate mean fluorescence intensity (means \pm SD, $n = 3$; * $P < 0.05$).

the BBB, accumulate in tumor sites and finally internalize into glioma cells upon linker cleavage by MMP-2 after Angiopep-2 modification.

3.6.3. CLSM

To investigate the cellular uptake profiles of micelles, CLSM was performed to analyze the cellular uptake of micelles/pEGFP-YOYO-1 in U251 cells at different time point. As shown in Fig. 4, the fluorescence intensity of pEGFP-YOYO-1 transfected by ch-K5(s-s)R8/pEGFP-YOYO-1 and ch-K5(s-s)R8-An/pEGFP-YOYO-1 was higher than that of pEGFP-YOYO-1 and bPEI-25K/pEGFP-YOYO-1 in U251 cells. Therefore, these CLSM images confirmed that pEGFP was simultaneously delivered into cells by the micelles, which is consistent with the result of the cellular uptake assay. In addition, after 1 h of incubation with micelles/pEGFP-YOYO-1, the red fluorescence (lysosomes) and pEGFP-YOYO-1 were overlapped. The yellow fluorescence, resulting from the overlay of red and green fluorescence in the merged image, indicated that pEGFP was effectively delivered into U251 cells. After 3 h of incubation, the green fluorescence was observed in the nuclear and perinuclear regions of the cytoplasm, indicating that pEGFP-YOYO-1 escaped from the endosome and entered the nucleus successfully.

3.7. Radiosensitization effects of ch-K5(s-s)R8-An/Dbait

3.7.1. CCK-8 assay

Cytotoxicity of ch-K5(s-s)R8-An/Dbait combined with radiation was investigated in U251 cells, in comparison with that of control,

ch-K5(s-s)R8-An and Dbait combined with radiation. As shown in Fig. 5A, an increase in the irradiation level produced a gradual decline in U251 cell viability. At a given irradiation dose, U251 cell viability was the lowest in ch-K5(s-s)R8-An/Dbait group. There was no significant difference between the control and the ch-K5(s-s)R8-An group, suggesting that ch-K5(s-s)R8-An exhibited no radiosensitization, and that the radiosensitization of ch-K5(s-s)R8-An/Dbait was derived from the Dbait. At a single irradiation dose of 2 Gy, the viability of U251 cells in the control, ch-K5(s-s)R8-An, Dbait and the ch-K5(s-s)R8-An/Dbait group was 94.07%, 89.29%, 81.35% and 72.90%, respectively. U251 cell viability was decreased significantly in ch-K5(s-s)R8-An/Dbait group at a low irradiation dose. This may be attributable to the sustained release of Dbait from ch-K5(s-s)R8-An/Dbait, and the enhanced cellular uptake of Dbait delivered by micelles.

3.7.2. Colony formation assay

Knowing that clonogenic assay or colony formation assay is an *in vitro* cell survival assay based on the ability of a single cell to form colony³⁷, we performed a clonogenic assay to determine the radiosensitization effect of ch-K5(s-s)R8-An/Dbait by cell growth inhibition. As shown in Fig. 5B, the plating efficiency in ch-K5(s-s)R8-An, Dbait and ch-K5(s-s)R8-An/Dbait groups without RT was similar to the control group, suggesting that they had no inhibitory effect on colony formation in U251 cells. In contrast, the plating efficiency of ch-K5(s-s)R8-An/Dbait+RT group was decreased significantly at 2 Gy and 4 Gy ($41.03 \pm 2.88\%$ and

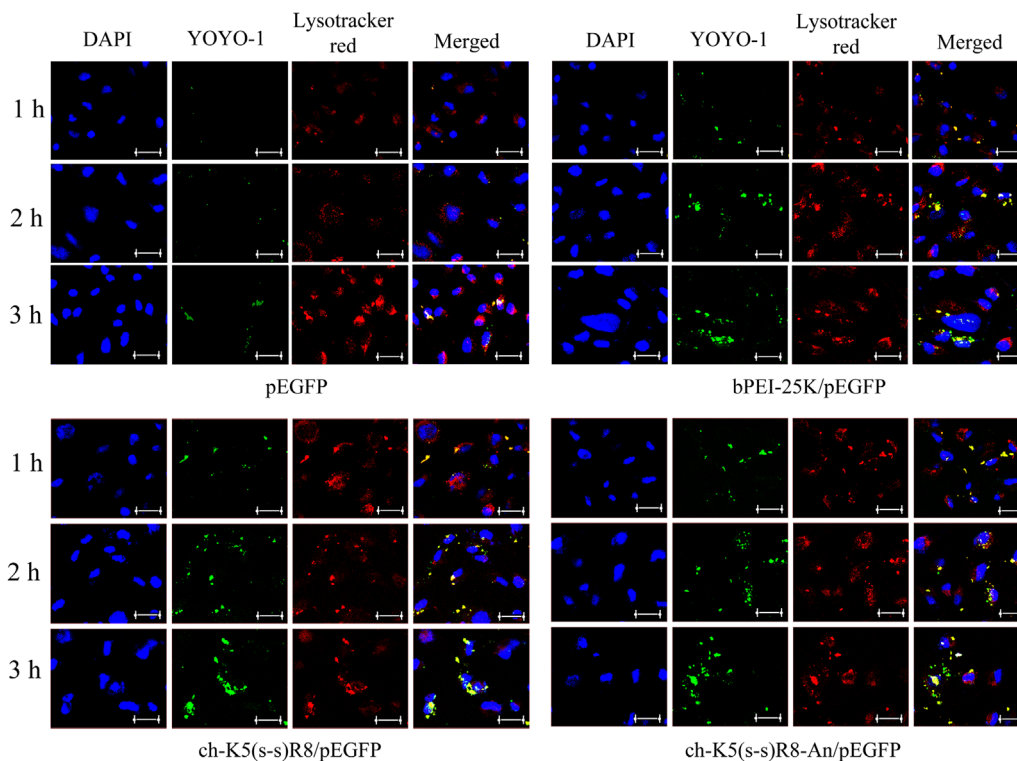


Figure 4 Cellular uptake analysis of micelles/pEGFP-YOYO-1 using CLSM, naked YOYO-1-labeled pEGFP (green) was used as blank control. U251 cells, with an incubation time of 1, 2 and 3 h, and Lysotracker Red was used to label the lysosomes. Scale bar, 20 μm .

$26.32 \pm 3.34\%$) as compared with the other groups ($P < 0.05$), suggesting that ch-K5(s-s)R8-An/Dbait+low-dose RT could effectively enhance the radiosensitization. In summary, the rapid internalization and sustained release of Dbait from micelles may substantially improve the anticancer effect of RT at the same dose. Knowing that high-dose RT would impair the cognitive function and other normal brain functions^{5,38}, we chose the low-dose (2 Gy) RT for the subsequent experiments.

3.7.3. Cell apoptosis assay

Apoptosis is an important indicator of DNA damage caused by ionizing radiation¹³. To investigate the effect of ch-K5(s-s)R8-An/Dbait + RT on the apoptosis of U251 cells, Annexin-V binding and PI staining assays were performed using a flow cytometer. U251 cells showed an early apoptosis level of 1.16% and a late apoptosis level of 1.10% in the control group (Fig. 5C). This type of apoptosis is normal for untreated cells since these cells would likely have undergone apoptosis under these growth conditions³⁷. The overall apoptosis rate in RT alone, ch-K5(s-s)R8-An+RT and Dbait+RT groups was $4.78 \pm 0.37\%$, $5.74 \pm 0.42\%$ and $8.15 \pm 0.28\%$ respectively vs. $15.72 \pm 0.53\%$ in ch-K5(s-s)R8-An/Dbait+RT group, confirming that the micelle combination of Dbait and RT was extremely effective in enhancing apoptosis of glioma cells and demonstrating the radiosensitizing effect of ch-K5(s-s)R8-An/Dbait.

3.7.4. Western blot analysis

In higher eukaryotic cells, the appearance of $\gamma\text{-H}_2\text{AX}$ in the cell nucleus is often used as an indicator of the presence of DNA DSBs^{39,40}. $\gamma\text{-H}_2\text{AX}$ foci are formed at DSB damage sites and resolved when the damage is repaired⁴¹. Therefore, we used Western blot analysis to see whether ch-K5(s-s)R8-An/Dbait +

RT could increase $\gamma\text{-H}_2\text{AX}$ in U251 cells. As shown in Fig. 6A, U251 cells treated with ch-K5(s-s)R8-An/Dbait + RT expressed significantly higher levels of $\gamma\text{-H}_2\text{AX}$ compared with non-treated cells. The level of $\gamma\text{-H}_2\text{AX}$ induced by ch-K5(s-s)R8-An/Dbait combined with 2 Gy RT was seven-fold higher than that induced by 2 Gy RT alone, and two times higher than that induced by Dbait+2 Gy RT (Fig. 6A and B). This suggests that the DNA repair ability of U251 cells was decreased after treatment with ch-K5(s-s)R8-An/Dbait+2 Gy RT.

We also examined the effect of ch-K5(s-s)R8-An/Dbait+2 Gy RT on other DNA repair proteins including DNA-PKcs and phospho-p53, and found that ch-K5(s-s)R8-An/Dbait+2 Gy RT also induced relatively high levels of DNA-PKcs and phospho-p53 in U251 cells (Fig. 6A, C and D). These results indicate that ch-K5(s-s)R8-An/Dbait + RT could inhibit DNA repair, which in turn improved the RT efficacy.

3.8. In vivo biodistribution

The ch-K5(s-s)R8/pEGFP-YOYO-1 and ch-K5(s-s)R8-An/pEGFP-YOYO-1 were injected intravenously into U251 orthotopic GBM-bearing nude mice to trace *in vivo* distribution and tumor-targeting characteristics. Fig. 7A shows the fluorescence intensity in the whole body at 1, 12, and 24 h after injection. The ch-K5(s-s)R8-An/pEGFP-YOYO-1 group (d) exhibited much stronger fluorescent signals and a directional aggregation ability at the brain tumor site as compared with the YOYO-1 (b) and ch-K5(s-s)R8/pEGFP-YOYO-1 (c) treated group, which displayed less fluorescence in the other organs tested. In the control group (b and c), YOYO-1 accumulated in other parts of the body. The excised organs were sectioned 24 h after injection to further study the *in vivo* micelle location. As shown in Fig. 7B, ch-K5(s-s)R8-

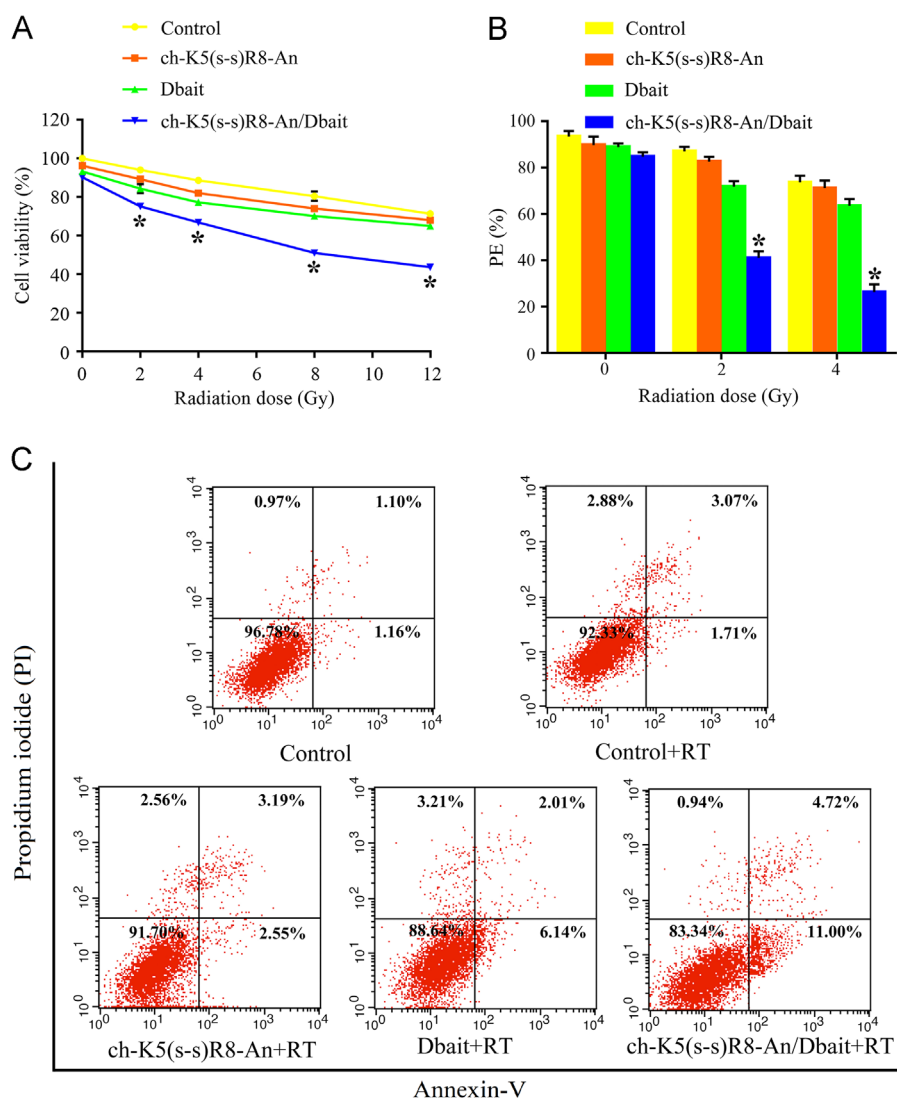


Figure 5 Radiosensitization effects of ch-K5(s-s)R8-An/Dbait. (A) Cell viability of U251 cells cultured with control, ch-K5(s-s)R8, fDbait and ch-K5(s-s)R8/Dbait for 6 h, and then treated with various doses of radiation. Cell viability were presented as mean \pm SD ($n = 3$). (B) PE of U251 cells cultured with control, ch-K5(s-s)R8, Dbait and ch-K5(s-s)R8/Dbait for 6 h, and then treated with various doses of radiation. PE were presented as mean \pm SD ($n = 3$). (C) Cell apoptosis of U251 cells induced by only RT, ch-K5(s-s)R8, Dbait and ch-K5(s-s)R8/Dbait combination with 2 Gy X-ray.

An/pEGFP-YOYO-1 (d) showed a high level of accumulation at the boundary and interior of the tumor; whereas YOYO-1 (b) and ch-K5(s-s)R8/pEGFP-YOYO-1 (c) accumulated mainly in the liver with less fluorescence in the brain. Thus, brain-targeting ch-K5(s-s)R8-An/pEGFP-YOYO-1 accumulation at the tumor site was markedly increased and the accumulation in the lungs, spleen, and other organs was substantially decreased. The results indicate that angiopep-2 modification could effectively enhance micelle accumulation in the tumor due to its positive brain-targeting characteristics.

3.9. *In vivo* toxicity assay

After staining with H&E (Fig. 7C), the images showed that the results of the heart, liver, spleen, lung, kidney and brain tissues in the group receiving blank ch-K5(s-s)R8-An micelles were similar to those of the PBS control group with no apparent inflammatory

response or damage being observed in any of the blank-micelle-treated group. This indicates that blank ch-K5(s-s)R8-An micelles had no obvious systemic toxicity.

4. Discussion

To overcome the insensitivity of glioma cells to RT, Dbait was used as a radiosensitizer to increase the sensitivity of U251 cells to RT. In the present study, we have developed a novel BBB and glioma dual-targeting and tumor microenvironment-responsive gene delivery system by using an MMP-2 responsive peptide as the enzymatically degradable linker to conjugate angiopep-2 and incorporated disulfide cross-linking in the middle shells to enhance cellular internalization and DNA release into the cytoplasm and nucleus.

Ch-Kn(s-s)R8-An forms core-shell-corona polymer micelles with three well-defined distinct domains: the inner hydrophobic

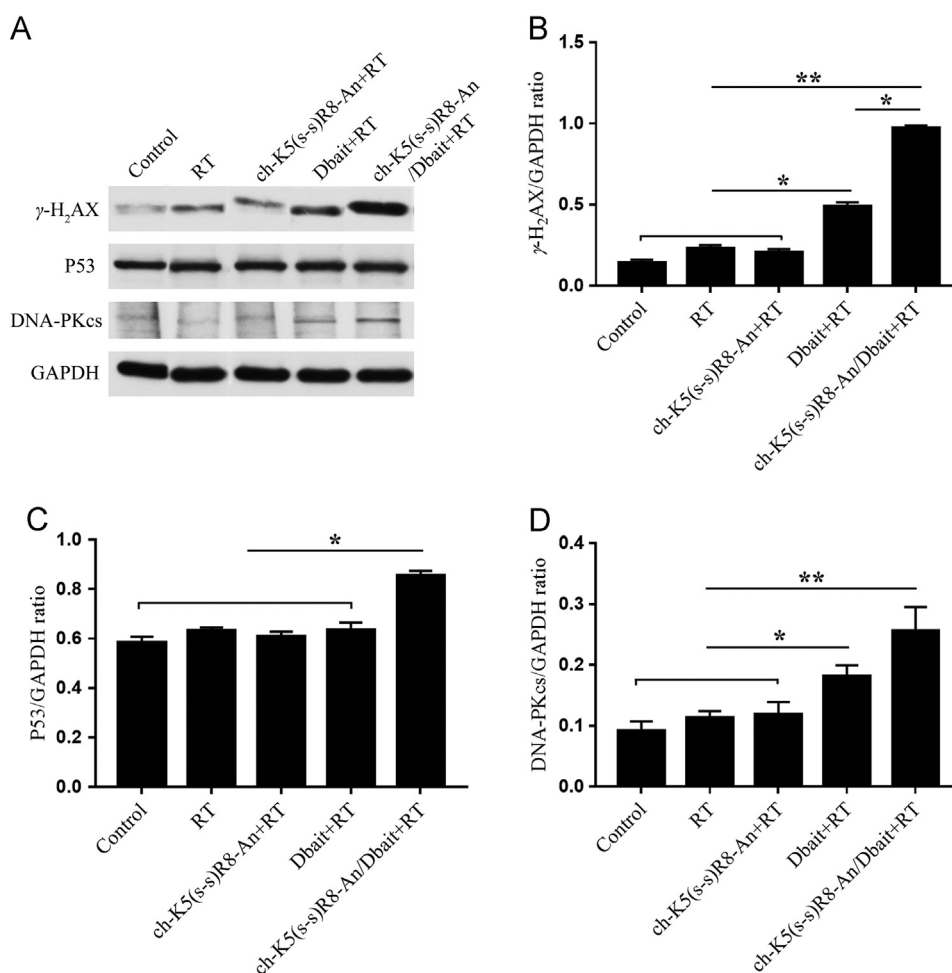


Figure 6 Western blot analysis of γ -H₂AX, DNA-PKcs and phospho-p53 protein levels in U251 cells. (A) Lysates of U251 cells were collected at 48 h after radiation for Western blot. The band intensity of γ -H₂AX (B), DNA-PKcs (C) and phospho-p53 (D) in U251 cells was quantified after normalized to GAPDH. Values were presented as mean \pm SD ($n = 3$).

cholesterol core, the cationic KnR8 middle shell, and the angiopep-2 targeting ligand in the outer corona. Successful disulfide cross-linking of ch-K n (s-s)R8-An was detected through the characteristic absorption peaks at 270 nm in UV spectra (Supporting Information Fig. S1). Cross-linking decreased the mean diameter of the micelles, indicating a condensed structure caused by chemical network formation in the micelle middle shells (Table 1). Notably, after cross-linking, the positive zeta potential of ch-K n R8 and ch-K n R8-An was decreased. This decreased zeta potential reflects the conversion of primary amine groups of the middle pLys shells to amide linkages³⁰. This result also demonstrated that the successful disulfide cross-linking of ch-K n (s-s)R8-An. As suggested previously, cross-linking could overcome the drawbacks of non-crosslinked micelles by decreasing the CMC of micelles, thus endowing them with more useful properties and performance for biomedical applications⁴². In the study, DTSSP was used as a disulfide-containing cross-linking agent to obtain the cross-linked micelles. The CMC results showed that the cross-linked micelles were compact and intact in an aqueous solution (Fig. 1C and D). The CMC values for non-crosslinked micelles increased gradually along with the lysine concentration increasing, probably due to the increased electrostatic repulsion between lysine moieties. However, the decrease in CMC values of cross-linked micelles with the amount of lysine increasing might be

caused by the higher degree of cross-linking. Furthermore, the particle size and zeta potential did not change significantly with the lapse of time in PBS (pH 7.4) with or without 10% FBS (Supporting Information Fig. S2). These results indicated that the cross-links in the middle shells may not only enhance the stability of micelles in the blood but reduce drug leakage before they reach the target tissue³⁰.

In this study, we have explored the possibility of gene delivery across the BBB by brain-targeted drug delivery system based on ch-K n (s-s)R8-An micelles to treat glioma. The rich external amine groups on the surface of micelles offer plenty reaction sites for functional modifications as well as positive charge for therapeutic gene encapsulation. The results of agarose gel electrophoresis suggest that disulfide cross-linked ch-K5(s-s)R8-An/pEGFP and ch-K7(s-s)R8-An/pEGFP were more stable, probably due to rich positive charges (Fig. 1G). In addition, ch-K n (s-s)R8-An/pEGFP ($n = 3, 5$ and 7) showed a weaker pEGFP binding affinity in a reducing environment (Fig. 1H). As reported, the reductive glutathione concentration in the cytosol of tumor cells was 100–1000 times higher than that in normal cells⁴³. Therefore, the presence of disulfide bonds may act as an effective means to maintain stability in the extracellular context and promote the release of the gene into tumor cells. In addition, the *in vitro* gene expression of different micelles/pEGFP in HEK293 and U251

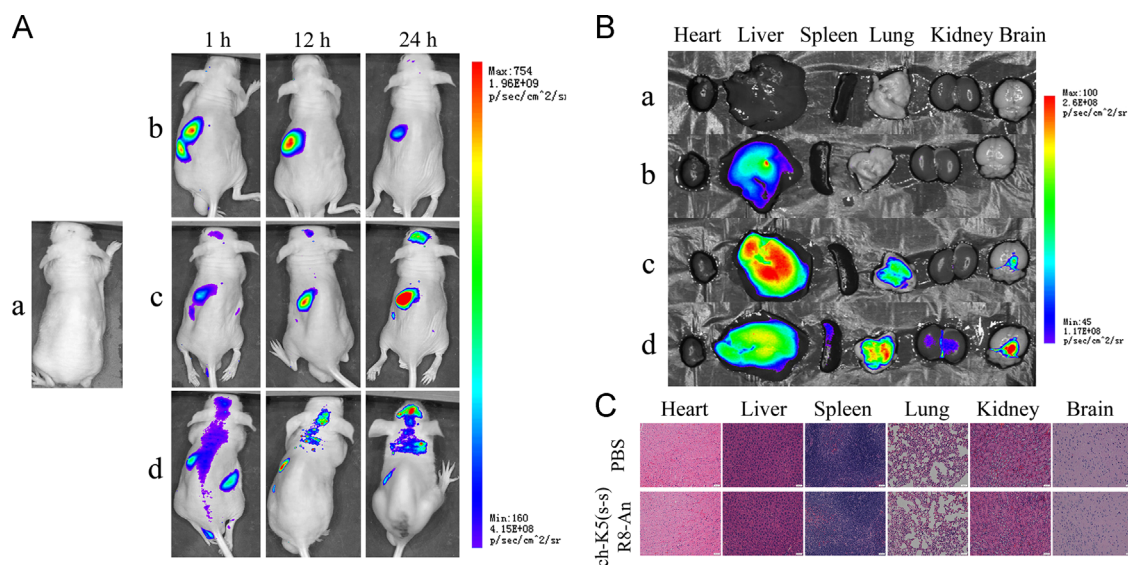


Figure 7 *In vivo* dynamic and specific distribution of micelles/pEGFP-YOYO-1. (A) Real-time *in vivo* fluorescence imaging of U251 tumor-bearing nude mice intravenously administrated with PBS (a), YOYO-1 (b), ch-K5(s-s)R8/pEGFP-YOYO-1 (c), and ch-K5(s-s)R8-An/pEGFP-YOYO-1 (d) at 1, 12, and 24 h at a dose of 50 mg pEGFP per mouse. (B) *Ex vivo* fluorescence images of dissected organs (heart, liver, spleen, lung, kidneys, and brain) of U251 tumor bearing nude mice sacrificed 24 h after intravenous injection of PBS (a), YOYO-1 (b), ch-K5(s-s)R8/pEGFP-YOYO-1 (c), and ch-K5(s-s)R8-An/pEGFP-YOYO-1 (d). (C) H&E histological staining of organs from mice injected with PBS and blank ch-K5(s-s)R8-An micelles. Scale bar, 50 μ m.

cells showed that ch-Kn(s-s)R8-An/pEGFP ($n = 5$ and 7) displayed an optimal gene transfection efficiency at an N/P ratio of 10, most probably because of enhanced gene compression (Fig. 2A–C).

According to previous reports⁴⁴, classical cationic polymers such as PEI generally exhibit a certain degree of heterogeneity because of the nature of the polymer chemistry. However, in the present study, ch-Kn(s-s)R8-An/pEGFP had more favorable biocompatibility with both cell lines than PEI (Fig. 2D and E). In addition, histological examination also indicated that the blank ch-K5(s-s)R8-An micelle had no significant systemic toxicity (Fig. 7C) which is consistent with the *in vitro* result. This benefit may derive from the micelles in the material, including cholesterol, lysine and arginine, all of which are known to have good biocompatibility as has been confirmed in clinical settings.

Angiopep-2 has been reported to play a key role in targeting the BBB and glioma^{18,45}. In this study, the angiopep-2 modified micelle entered the cells much more efficiently in BCECs but not in HEK293 cells, compared with the angiopep-2 non-modified micelle (Fig. 3). In addition, BBB penetration of Angiopep-2 modified micelle treated with MMP-2 was significantly enhanced. Linker MMP-2 responsive peptides are broken in the presence of MMP-2 to expose the R8. This simultaneously reduces the particle size and drives the micelles into glioma cells with up-regulated MMP-2. Non-modified micelles with an R8 shell exhibited the ability to penetrate the cell membrane. However, without tumor targeting and selectivity, the R8 shell had lower cellular uptake into tumor cells *in vivo*⁴⁶. For example, CPPs initially binds to the local vasculature and redistributes to the liver after intravenous administration, where more than 90% of the injected dose accumulates after 30 min⁴⁷. In this study, non-modified micelles accumulated mainly in the liver with less fluorescence in the brain. It is probably that long-circulating decoration helps to divert a fraction of nanoparticles to peripheral tissues, but a large fraction of nanoparticles are still captured by the macrophage-rich

organs^{48,49}. In addition, these results indicate that modification of angiopep-2 played a role in targeting the BBB, and that cleavage of angiopep-2 subsequently enhanced internalization in tumor cells. Also, the *in vivo* imaging results provided convincing evidence that this tumor-triggered mechanism makes the delivery system increase the pDNA content at the glioma site and decrease the pDNA content in the macrophage-rich organs such as liver (Fig. 7A and B).

In our study, ch-K5(s-s)R8-An was used as a delivery nanocarrier to transport the radiosensitizer Dbait to U251 cells. A previous study reported by Yao et al.⁴¹ showed that upon irradiation, the Dbait molecule could further improve the RT efficacy for PCA cell lines. For the first time, we demonstrated that ch-K5(s-s)R8-An/Dbait+RT was able to increase the sensitivity of U251 cells to RT, inhibited colony formation in U251 cells, and promoted cell apoptosis (Fig. 5). Moreover, Western blot analysis showed that ch-K5(s-s)R8-An/Dbait + RT inhibited the DNA damage repair signaling pathway by mimicking DNA double-strand breaks (Fig. 6), which is consistent with previous studies⁴¹. Thereby, ch-K5(s-s)R8-An/Dbait combined with RT exerts a strong antitumor phenotype by impairment of proliferation and induction of apoptosis in tumor cells.

5. Conclusions

In summary, we have developed a novel dual-targeting and microenvironment-responsive micelle (ch-Kn(s-s)R8-An/pDNA) for gene delivery during glioma treatment. The microenvironment-responsive micelles showed higher gene transfection efficiency, improved brain-penetrating and glioma-targeting efficiency, better biocompatibility and improved therapeutic efficacy during glioma radiotherapy *in vitro*. *In vivo* study also demonstrated good micelle-glioma targeting with no obvious toxicity toward normal tissues. All these results demonstrate the tremendous potential of this tumor-

triggered micelle system for efficient delivery of gene therapeutic agents during oncotherapy. Further work will focus on investigation and development of ch-K5(s-s)R8-An/Dbait as a radiosensitizer in glioma treatment *in vivo*.

Acknowledgments

We acknowledge the financial support received from the National Natural Science Foundation of China (No. 81472349, 81302714 and 81201809, China); the Natural Science Foundation of Shanghai (No. 14ZR1433300, China); the Interdisciplinary Program of Shanghai Jiao Tong University (No. 0507N17014, China); the Innovation Program of Shanghai Municipal Education Commission (No. 15ZZ041, China); Natural Science Foundation of Zhejiang Province (No. LQ12H30005, China); and the Public Welfare Technology Application Research Project (No. LGF18H160034, China).

Appendix A. Supporting information

Supplementary data associated with this article can be found in the online version at <https://doi.org/10.1016/j.apsb.2018.12.001>.

References

- Alifieris C, Trafalis DT. Glioblastoma multiforme: pathogenesis and treatment. *Pharmacol Ther* 2015;**152**:63–82.
- Zhang M, Lu W. Enhanced glioma-targeting and stability of ¹GICP peptide coupled with stabilized peptide ^DA7R. *Acta Pharm Sin B* 2018;**8**:106–15.
- Donahue MJ, Blakeley JO, Zhou J, Pomper MG, Larterra J, van Zijl PC. Evaluation of human brain tumor heterogeneity using multiple T₁-based MRI signal weighting approaches. *Magn Reson Med* 2008;**59**:336–44.
- Dutreix M, Cosset JM, Sun JS. Molecular therapy in support to radiotherapy. *Mutat Res* 2010;**704**:182–9.
- Saad S, Wang TJ. Neurocognitive deficits after radiation therapy for brain malignancies. *Am J Clin Oncol* 2015;**38**:634–40.
- Zhao X, Chen R, Liu M, Feng J, Chen J, Hu K. Remodeling the blood–brain barrier microenvironment by natural products for brain tumor therapy. *Acta Pharm Sin B* 2017;**7**:541–53.
- Li J, Guo Y, Kuang Y, An S, Ma H, Jiang C. Choline transporter-targeting and co-delivery system for glioma therapy. *Biomaterials* 2013;**34**:9142–8.
- Biau J, Devun F, Verrelle P, Dutreix M. Dbait: an innovative concept to inhibit DNA repair and treat cancer. *Bull Cancer* 2016;**103**:227–35.
- Coquery N, Pannetier N, Farion R, Herbet A, Azurmendi L, Clarencon D, et al. Distribution and radiosensitizing effect of cholesterol-coupled Dbait molecule in rat model of glioblastoma. *PLoS One* 2012;**7**:e40567.
- Devun F, Biau J, Huerre M, Croset A, Sun JS, Denys A, et al. Colorectal cancer metastasis: the DNA repair inhibitor Dbait increases sensitivity to hyperthermia and improves efficacy of radiofrequency ablation. *Radiology* 2014;**270**:736–46.
- Quanz M, Berthault N, Roulin C, Roy M, Herbet A, Agrario C, et al. Small-molecule drugs mimicking DNA damage: a new strategy for sensitizing tumors to radiotherapy. *Clin Cancer Res* 2009;**15**:1308–16.
- Biau J, Devun F, Jdey W, Kotula E, Quanz M, Chautard E, et al. A preclinical study combining the DNA repair inhibitor Dbait with radiotherapy for the treatment of melanoma. *Neoplasia* 2014;**16**:835–44.
- Liu H, Cai Y, Zhang Y, Xie Y, Qiu H, Hua L, et al. Development of a hypoxic radiosensitizer-prodrug liposome delivery DNA repair inhibitor dbait combination with radiotherapy for glioma therapy. *Adv Healthc Mater* 2017 Available from: <https://doi.org/10.1002/adhm.201601377>.
- Visser CC, Voorwinden LH, Crommelin DJ, Danhof M, de Boer AG. Characterization and modulation of the transferrin receptor on brain capillary endothelial cells. *Pharm Res* 2004;**21**:761–9.
- Liu C, Liu XN, Wang GL, Hei Y, Meng S, Yang LF, et al. A dual-mediated liposomal drug delivery system targeting the brain: rational construction, integrity evaluation across the blood–brain barrier, and the transporting mechanism to glioma cells. *Int J Nanomed* 2017;**12**:2407–25.
- Demeule M, Currie JC, Bertrand Y, Ché C, Nguyen T, Régina A, et al. Involvement of the low-density lipoprotein receptor-related protein in the transcytosis of the brain delivery vector angiopep-2. *J Neurochem* 2008;**106**:1534–44.
- Huang S, Li J, Han L, Liu S, Ma H, Huang R, et al. Dual targeting effect of angiopep-2-modified, DNA-loaded nanoparticles for glioma. *Biomaterials* 2011;**32**:6832–8.
- Ruan S, Yuan M, Zhang L, Hu G, Chen J, Cun X, et al. Tumor microenvironment sensitive doxorubicin delivery and release to glioma using angiopep-2 decorated gold nanoparticles. *Biomaterials* 2015;**37**:425–35.
- Kang L, Gao Z, Huang W, Jin M, Wang Q. Nanocarrier-mediated co-delivery of chemotherapeutic drugs and gene agents for cancer treatment. *Acta Pharm Sin B* 2015;**5**:169–75.
- Huang WC, Chen SH, Chiang WH, Huang CW, Lo CL, Chern CS, et al. Tumor microenvironment-responsive nanoparticle delivery of chemotherapy for enhanced selective cellular uptake and transportation within tumor. *Biomacromolecules* 2016;**17**:3883–92.
- Liu Y, Zhang D, Qiao ZY, Qi GB, Liang XJ, Chen XG, et al. A peptide-network weaved nanoplatform with tumor microenvironment responsiveness and deep tissue penetration capability for cancer therapy. *Adv Mater* 2015;**27**:5034–42.
- Feng Q, Shen Y, Fu Y, Muroski ME, Zhang P, Wang Q, et al. Self-assembly of gold nanoparticles shows microenvironment-mediated dynamic switching and enhanced brain tumor targeting. *Theranostics* 2017;**7**:1875–89.
- MacEwan SR, Chilkoti A. Applications of elastin-like polypeptides in drug delivery. *J Control Release* 2014;**190**:314–30.
- Kato T, Yamashita H, Misawa T, Nishida K, Kurihara M, Tanaka M, et al. Plasmid DNA delivery by arginine-rich cell-penetrating peptides containing unnatural amino acids. *Bioorg Med Chem* 2016;**24**:2681–7.
- Cui Y, Sui J, He M, Xu Z, Sun Y, Liang J, et al. Reduction-degradable polymeric micelles decorated with parg for improving anticancer drug delivery efficacy. *ACS Appl Mater Interfaces* 2016;**8**:2193–203.
- Vivès E, Schmidt J, Pèlegri A. Cell-penetrating and cell-targeting peptides in drug delivery. *Biochim Biophys Acta* 2008;**1786**:126–38.
- Fonseca SB, Pereira MP, Kelley SO. Recent advances in the use of cell-penetrating peptides for medical and biological applications. *Adv Drug Deliv Rev* 2009;**61**:953–64.
- Huang S, Shao K, Kuang Y, Liu Y, Li J, An S, et al. Tumor targeting and microenvironment-responsive nanoparticles for gene delivery. *Biomaterials* 2013;**34**:5294–302.
- Yao C, Tai Z, Wang X, Liu J, Zhu Q, Wu X, et al. Reduction-responsive cross-linked stearyl peptide for effective delivery of plasmid DNA. *Int J Nanomed* 2015;**10**:3403–16.
- Koo AN, Min KH, Lee HJ, Lee SU, Kim K, Kwon IC, et al. Tumor accumulation and antitumor efficacy of docetaxel-loaded core-shell-corona micelles with shell-specific redox-responsive cross-links. *Biomaterials* 2012;**33**:1489–99.
- Shao K, Zhang Y, Ding N, Huang S, Wu J, Li J, et al. Functionalized nanoscale micelles with brain targeting ability and intercellular microenvironment biosensitivity for anti-intracranial infection applications. *Adv Healthc Mater* 2015;**4**:291–300.
- Huang J, Zhang H, Yu Y, Chen Y, Wang D, Zhang G, et al. Biodegradable self-assembled nanoparticles of poly(D,L-lactide-co-glycolide)/hyaluronic acid block copolymers for target delivery of docetaxel to breast cancer. *Biomaterials* 2014;**35**:550–66.

33. Kim JS, Oh MH, Park JY, Park TG, Nam YS. Protein-resistant, reductively dissociable polyplexes for *in vivo* systemic delivery and tumor-targeting of siRNA. *Biomaterials* 2013;**34**:2370–9.
34. Mann A, Shukla V, Khanduri R, Dabral S, Singh H, Ganguli M. Linear short histidine and cysteine modified arginine peptides constitute a potential class of DNA delivery agents. *Mol Pharm* 2014;**11**:683–96.
35. Zhang D, Wang J, Xu D. Cell-penetrating peptides as noninvasive transmembrane vectors for the development of novel multifunctional drug-delivery systems. *J Control Release* 2016;**229**:130–9.
36. Cai H, Liang Z, Huang W, Wen L, Chen G. Engineering PLGA nano-based systems through understanding the influence of nanoparticle properties and cell-penetrating peptides for cochlear drug delivery. *Int J Pharm* 2017;**532**:55–65.
37. Ding B, Wahid MA, Wang Z, Xie C, Thakkar A, Prabhu S, et al. Triptolide and celastrol loaded silk fibroin nanoparticles show synergistic effect against human pancreatic cancer cells. *Nanoscale* 2017;**9**:11739–53.
38. McDuff SG, Taich ZJ, Lawson JD, Sanghvi P, Wong ET, Barker II FG, et al. Neurocognitive assessment following whole brain radiation therapy and radiosurgery for patients with cerebral metastases. *J Neurol, Neurosurg, Psychiatry* 2013;**84**:1384–91.
39. Giovannini C, Piaggi S, Federico G, Scarpato R. High levels of γ -H2AX foci and cell membrane oxidation in adolescents with type 1 diabetes. *Mutat Res* 2014;**770**:128–35.
40. Gonzalez JE, Roch-Lefèvre SH, Mandina T, Garcia O, Roy L. Induction of γ -H2AX foci in human exfoliated buccal cells after *in vitro* exposure to ionising radiation. *Int J Radiat Biol* 2010;**86**:752–9.
41. Yao H, Qiu H, Shao Z, Wang G, Wang J, Yao Y, et al. Nanoparticle formulation of small DNA molecules, Dbait, improves the sensitivity of hormone-independent prostate cancer to radiotherapy. *Nanomed: Nanotechnol, Biol, Med* 2016;**12**:2261–71.
42. Huang L, Liu M, Mao L, Zhang X, Xu D, Wan Q, et al. Polymerizable aggregation-induced emission dye for preparation of cross-linkable fluorescent nanoprobes with ultra-low critical micelle concentrations. *Mater Sci Eng C, Mater Biol Appl* 2017;**76**:586–92.
43. Cheng R, Feng F, Meng F, Deng C, Feijen J, Zhong Z. Glutathione-responsive nano-vehicles as a promising platform for targeted intracellular drug and gene delivery. *J Control Release* 2011;**152**:2–12.
44. Klein PM, Müller K, Gutmann C, Kos P, Krhac Levacic A, Edinger D, et al. Twin disulfides as opportunity for improving stability and transfection efficiency of oligoaminoethane polyplexes. *J Control Release* 2015;**205**:109–19.
45. Velasco-Aguirre C, Morales-Zavala F, Salas-Huenuleo E, Gallardo-Toledo E, Andonie O, Muñoz L, et al. Improving gold nanorod delivery to the central nervous system by conjugation to the shuttle angiopep-2. *Nanomedicine* 2017;**12**:2503–17.
46. Yang D, Yang X, Lee RJ, Liu S, Xie J. Liposomes incorporating transferrin and stearic acid-modified octa-arginine for siRNA delivery. *Anticancer Res* 2017;**37**:1759–64.
47. Aguilera TA, Olson ES, Timmers MM, Jiang T, Tsien RY. Systemic *in vivo* distribution of activatable cell penetrating peptides is superior to that of cell penetrating peptides. *Integr Biol* 2009;**1**:371–81.
48. He H, Zhang J, Xie Y, Lu Y, Qi J, Ahmad E, et al. Bioimaging of intravenous polymeric micelles based on discrimination of integral particles using an environment-responsive probe. *Mol Pharm* 2016;**13**:4013–9.
49. He H, Jiang S, Xie Y, Lu Y, Qi J, Dong X, et al. Reassessment of long circulation *via* monitoring of integral polymeric nanoparticles justifies a more accurate understanding. *Nanoscale Horiz* 2018;**3**:397–407.